Influence of emissivity tailoring on radiative membranes thermal behavior for gas sensing applications

Anthony Lefebvre, Daniele Costantini, Giovanni Brucoli, Salim Boutami, Jean-Jacques Greffet, Henri Benisty

Influence of emissivity tailoring on radiative membranes thermal behavior for gas sensing applications

Anthony Lefebvre [a,b,*], Daniele Costantini [b], Giovanni Brucoli [b], Salim Boutami [a], Jean-Jacques Greffet [b], Henri Benisty [b]

[a] Univ Grenoble Alpes F-38000 Grenoble, France, CEA, LETI, MINATEC Campus, F-38054 Grenoble, France
[b] Laboratoire Charles Fabry, Institut d'Optique, CNRS, Univ Paris Sud, 2, Avenue Augustin Fresnel, 91127 Palaiseau cedex, France

Suspended micro-hotplates acting as infrared emitting sources are privileged energy-efficient sources for intended use in optical gas sensors. For such sources, the main constraints are the maximum operating temperature and the battery-limited available energy per measurement. Using simulations that take into account the dynamics of heating through the spatio-temporal radial profile, we first demonstrate how to design a thermally efficient membrane complying with these specifications. Once nonspecific thermal leaks are minimized, we show a further increase of the wall-plug efficiency by tailoring the membrane spectral emissivity with a metasurface in order to match the absorption spectrum of a gas of interest, e.g. CO_2 in this study. We consider the effects of an array of plasmonic resonators on the overall efficiency, and show non-trivial favorable effects on the thermal balance of the system.

1. Introduction

Optical gas sensors have many advantages when compared to competing approaches such as metal-oxide-semiconductor, catalytic or electrochemical sensors: they achieve high sensitivity and selectivity, they have virtually unlimited lifetime and they are not subject to poisoning [1]. The only drawback is their price, which arises from their relative complexity. In these sensors, one measures the transmission of infrared (IR) radiation emitted by a dedicated source through the gas of interest. Due to the unique molecular absorption fingerprint exhibited by most gases in the IR range, the power attenuation measured by a detector provides the gas concentration according to Beer-Lambert law:

$$P = \int_{\Delta\lambda} P_0(\lambda) 10^{-\varepsilon_{\mathrm{mol}}(\lambda) l c} d\lambda \tag{1}$$

where P is the measured power, $P_0(\lambda)$ is the reference spectral power in the absence of gas, l is the path length through the gas, and ϵ_{mol} and c are respectively the molar absorptivity and concentration of the gas. The sensitivity of the measurement depends on the signal-to-noise ratio, while its reliability depends on the cross-talk caused by interfering gases in the targeted line. The detector is e.g. a pyroelectric sensor, a thermopile or a bolometer. The source is either a quantum cascade laser for high-cost/high-precision sensors, or a blackbody-like source in cheaper devices. In this case, it is often designed as a suspended microbridge, micromembrane or microhotplate, using Micro-Electro-Mechanical Systems (MEMS) technology. This allows the source to be thermally insulated from the substrate, increasing its efficiency. Although these structures were first demonstrated in the 1980s [2,3], a lot of work is still in progress on this topic, particularly regarding temperature homogeneity [4–6]. Ali et al. provided an extensive review of latest achievements concerning micromembranes [7].

Although increasing the temperature of the membrane is the easiest way to improve the dominance of radiative flux over other losses (conduction, convection), there is an upper limit set by technological constraints in order to avoid premature degradation. The device lifetime is mostly limited by electromigration effects likely to disrupt conductive paths, and by thermomechanical fatigue, leading to arm's rupture. The former are avoided by limiting the current density in the conductive tracks, while the latter depends

* Corresponding author. Tel.: +33 438784094.
E-mail address: anthony.lefebvre@cea.fr (A. Lefebvre).

on the membrane thermal expansion [8]. Thermal deformations can be lessened using non axisymmetric suspension arms, used for example in bolometers [9]. The source is thus operated at this limit temperature in the following calculations. In order to design a battery-powered, long-lasting, efficient source, available energy is restricted for each measurement. As a result, dynamics matter: a basic trend is for instance that the larger the membrane, the more power it demands, and the shorter the time it can be powered on before the allocated energy is exhausted. It turns out that getting the best detection under such constraints is no simple design exercise. In the following, we show how to find the best compromise in order to maximize the wall-plug efficiency for the detection of a specific gas, with the CO_2 example in mind. We also give an insight into the thermo-optical mechanisms governing this kind of devices, and the influence of emissivity tailoring on overall efficiency. Practical figures are given for a 5 mJ allocated energy per measurement, and a 650 °C maximum membrane temperature, corresponding to a realistic, low-consumption gas sensor discussed in more details in Section 3.

2. Modeling

We consider a rather generic wafer-level suspended microhotplate, for example the one developed by Barritault et al. [10], shown in Fig. 1a, made of resistive metallic tracks inside a dielectric ring-shaped shell in a series/parallel arrangement (clear wire-like areas in Fig. 1a). Heating is achieved via Joule effect, and the rather narrow mechanical suspension reduces thermal losses to the substrate. Temperature homogeneity inside the disc is guaranteed by the use of electrically isolated heat-spreading areas surrounding the heating wires and made of the same stack. In order to reduce computation time and to retain generality, we consider a model (Fig. 1b) based on three straightforward simplifications:

- The membrane thickness is much smaller than the central disk radius, implying that the heat distribution is constant along the vertical axis.
- The central disk of radius R consists of a single material, due to the presence of heat-spreading spacers actually made of the same stack of materials as the wires, covering most of the disk.
- The system is modeled as fully axisymmetric: even the arms can be homogenized around the central disk, considering effective thermal conduction characteristics based on the relative fraction of their intersection with the perimeter of the membrane. Their outer boundary at radius R_{out} can be also considered as thermalized with the substrate holding the membrane. Metallic tracks azimuthal dependence is neglected. The trends we find should not be sizably affected by this level of detail.

The obtained one-dimensional bi-material model associated to a variable r in the interval $[0,R_{\text{out}}]$ is illustrated on Fig. 1b.

Let us now treat this model: a subsequent approximation that holds for most reasonable combination of the above choices is that the arms contribution to the overall radiative flux is negligible due to their small surface and low temperature. As a consequence, they can be considered as a simple thermal leakage resistance Z_{a}, defined by:

$$Z_a = \frac{L_a}{k'_a} = \frac{L_a}{k_a \dfrac{N_a w_a}{2\pi R}} \quad [\text{K.W}^{-1}.\text{m}^2] \tag{2}$$

where N_{a}, L_{a} and w_{a} are respectively the number, length and inner arc width of the arms and k'_a is the equivalent thermal conductivity, obtained from the arms thermal conductivity k_a weighted by the relative fraction of their subtended inner arc with the perimeter of the membrane, $N_{\text{a}}w_{\text{a}}/2\pi R$. In the following calculations, Z_{a} is kept constant by increasing the inner arc width of the arms w_a at the same rate as the radius of the membrane, and keeping their length unchanged. One can check that this is a consistent way to preserve the mechanical resistance of the structure. Heat equations are then expressed as:

$$\rho C_p \frac{\partial T(r,t)}{\partial t} = k\left[\frac{\partial^2 T(r,t)}{\partial r^2} + \frac{1}{r}\frac{\partial T(r,t)}{\partial r}\right] - \frac{1}{e}\left\{\varphi_{\text{rad}_{\text{top}}}[T(r,t)] + \varphi_{\text{rad}_{\text{bot}}}[T(r,t)]\right\} + P(r,t) \tag{3}$$

with

$$\varphi_{\text{rad}_{\text{top/bot}}}[T(r,t)] = \pi \int_0^\infty \varepsilon_{\text{top/bot}}(\lambda)\{I[\lambda, T(r,t)] - I(\lambda, T_{\text{sub}})\}d\lambda \tag{4}$$

where ρ is the mass density, C_{p} is the specific heat capacity, k is the thermal conductivity, $\varepsilon_{\text{top/bot}}$ is the emissivity of the top or bottom surface of the membrane, and I stands for the spectral radiance of the blackbody, given by Planck's law. Convection losses are neglected as the source is encapsulated under vacuum. The source power $P(r,t)$ is constant over the central disk of the membrane (practically, this assumption depends on the exact wire pattern, and boils down to a tractable electrical problem). Initially, the whole membrane is at the substrate temperature T_{sub} and the model's boundary conditions are given by:

$$-k\frac{\partial T(0,t)}{\partial r} = 0 \tag{5}$$

$$-k\frac{\partial T(R,t)}{\partial r} = \frac{1}{Z_a e}(T(R,t) - T_{sub}) \tag{6}$$

Eq. (5) comes from the axisymmetry, and Eq. (6) is a Robin condition taking into account the arms thermal resistance (with T_{sub} the substrate temperature being the actual boundary condition at the attached end of the arms). From the computed spatio-temporal temperature profile, we define the efficiency of the source as the ratio of the energy $E_{\text{rad,top}}$ radiated by the top surface over the total energy (radiated and conducted E_{cond} to the substrate):

$$\eta = \frac{E_{\text{rad,top}}}{E_{\text{rad,bot}} + E_{\text{rad,top}} + E_{\text{cond}}} \tag{7}$$

with

$$E_{\text{cond}} = \int_0^{t_f} \frac{(T(R,t) - T_{\text{sub}})}{Z_a} N_a w_a e dt \tag{8}$$

and

$$E_{\text{rad,top/bot}} = \pi \int_0^{t_f}\int_0^{R}\int_0^{\infty} \varepsilon_{\text{top/bot}}(\lambda)[I(\lambda, T(r,t)) - I(\lambda, T_{\text{sub}})]\text{d}\lambda\, r\text{d}r\, \text{d}t \tag{9}$$

where t_f is a long time at which we consider that the membrane is back to the substrate temperature. In the case of a blackbody, $\varepsilon_{\text{top}} = \varepsilon_{\text{bot}} = 1$, which is not very favorable as all the radiation emitted by the bottom surface is lost in this model. We shall also define a spectral efficiency η_λ akin to Eq. (7) but taking into account only the radiation in a specific wavelength range in Eq. (9).

3. Case study

3.1. Blackbody emitter

In order to demonstrate the main results of this study, we model a membrane similar to the one developed by Barritault et al. [10].

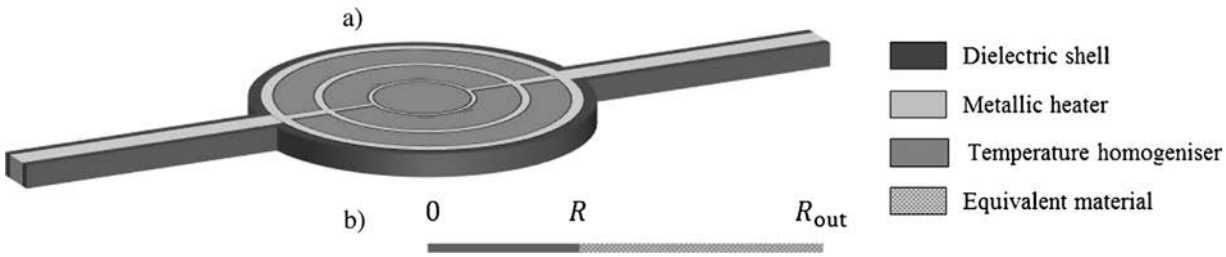

Fig. 1. (a) Membrane illustration, (b) simplified 1D model.

It consists of a metallic TiN(10 nm)/Pt(30 nm)/TiN(10 nm) tri-layer embedded into two 100 nm thick Si_3N_4 layers. Extra deposited TiN layers sandwiching Pt act as diffusion barriers for this metal. A 100 nm thick SiO_2 layer is used to manage the mechanical constraints inside the stack and avoid the buckling of the membrane. The total thickness of the structure is $e = 350$ nm. Our default radius is $R = 75\ \mu m$ ($R \gg e$), and the structure is suspended by $N_a = 2$ arms of length $L_a = 150\ \mu m$ and width $w_a = 30\ \mu m$. The thermal resistivity of the arms is $Z_a = 1.5\ 10^{-4}\ K W^{-1}\ m^2$. Physical properties of the materials are summarized in Table 1.

This membrane has been shown to operate with very little degradation up to $T_f = 650\ ^\circ C$ [16], which will thus be our operating temperature. Concerning the available energy per measurement, using a standard 1.5V AA battery (2.6Wh, or 9360 J), a 10 years expected lifetime and 3 min repetition rate, we must limit the energy per measurement to $E = 5$ mJ. The gas of interest is carbon dioxide (CO_2), which has a strong absorption feature between 4.16 and 4.36 μm, defining the window over which spectral efficiency is computed. CO_2 becomes a health hazard above 1000 ppm, the normal level being ∼400 ppm in atmosphere in 2014. Its monitoring is thus needed for air quality control, in meeting rooms or public spaces for instance.

Eqs. (3)–(6) are implemented in a Matlab routine, matching different heating times t_h to corresponding membrane radius R in such a way that the system complies with the above specifications: the differential equation is solved with such constraints with the existing package, even though they are not usual boundary conditions. This way, a $R(t_h)$ law is found, and spectral efficiencies are computed using Eqs. (7)–(9) along this line. Fig. 2 presents the results obtained as a series of dots whose color indicates the obtained spectral efficiency in the (t_h,R) parameter space, constrained by $E = 5$ mJ and $T_f = 650\ ^\circ C$.

Different regimes can be observed on this figure:

- At short heating times ($t_h < 10$ ms), the curve approaches a horizontal asymptote around $R = 1500\ \mu m$. In this case all the available energy is used to raise the temperature of the large radius membrane, before any kind of loss can happen. The energy being limited, the maximum radius can be computed from $E = \pi R^2 e \rho C_p (T_f - T_{sub})$. However, these configurations require very high power, as $P = E/t$. The use of a specific power source or supercapacitor buffer may thus be necessary, which can be prohibitive when standard batteries are desired (ceiling applications similar to smoke detectors are envisioned, for instance).
- For longer heating times ($t_h > 10$ ms, the membrane is almost operated in steady state, and the supplied power compensates the losses. These losses can be separated between conductive and radiative ones, and give rise to two different regimes:
  - When radiative losses are prominent ($10\ ms < t_h < 10\ s$), losses scale with R^2, and the logarithmic curve is linear with a slope defined by $R^2 t_h = $ constant.
  - When conductive losses are prominent ($t_h > 10$), losses scale with R, and the logarithmic curve becomes linear with a slope defined by $R t_h = $ constant. This regime is not shown in Fig. 2 as it is far from our heating time range of interest.

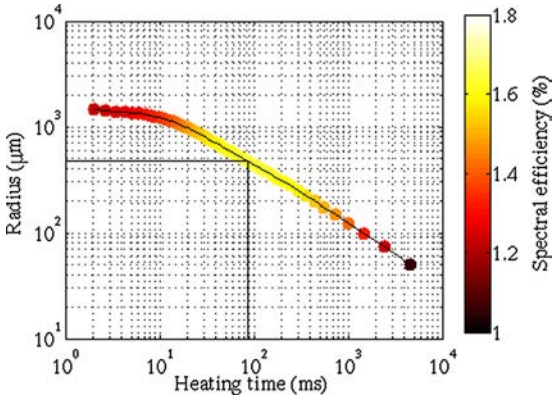

Fig. 2. $R(t_h)$ radius-duration solutions of the constrained thermal equations with $E = 5$ mJ and $T_f = 650\ ^\circ C$ and corresponding spectral efficiency (color). Black lines at 85 ms and 475 μm indicate the optimum.

From these results, we can see that the best CO_2-band spectral efficiency is about 1.6%, and is achieved for $R = 475\ \mu m$ and $t_h = 85$ ms. These values yield the best compromise between the radius of the membrane, and the time it can be heated. However, even this maximum efficiency is quite low, and one may wonder why we get such a value on the order of a few percent. This is simply due here to the strong mismatch between the sharp CO_2 spectral

Table 1
Material physical properties at room temperature (300 K). Temperature dependence is neglected.

	Thickness (nm)	Density (kg m^{-3})	Specific heat capacity (J kg^{-1} K^{-1})	Thermal conductivity (W m^{-1} K^{-1})
Materials of model membrane				
Si_3N_4	200	3100 [11]	700 [11]	2.6 [12]
SiO_2	100	2200 [11]	1000 [11]	1.2 [12]
TiN	20	5400 [13]	545 [13]	19.2 [13]
Pt	30	21450 [14]	131 [14]	58 [12]
Total/Weighted mean	350	4547	728	7.9
Material of MIM study				
W	100	19250[15]	130[15]	175[15]

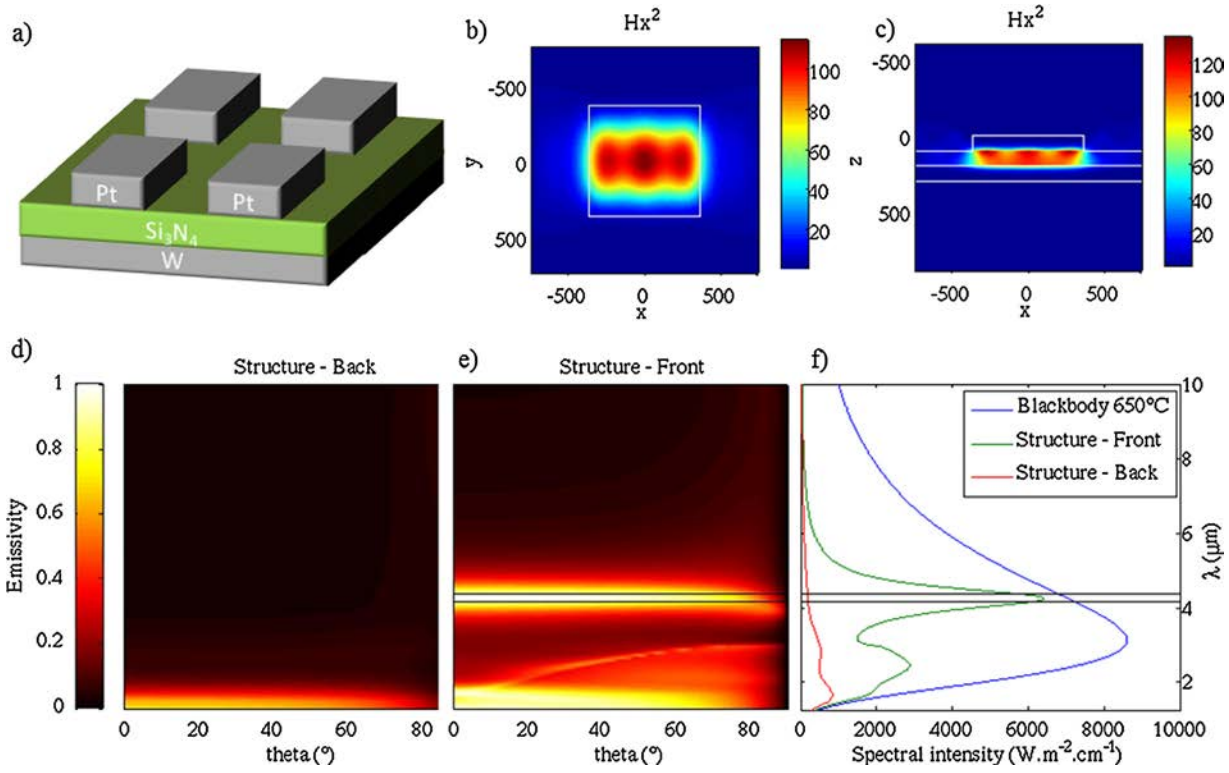

Fig. 3. (a) The chosen MIM structure, with square Pt patches; (b) and (c) Field maps in the *xy* and *xz* planes; (d) and (e) RCWA-computed emissivity versus angle and wavelength for the front and back side of the structure; (f) corresponding spectral intensities integrated on a hemisphere for $T_f = 650\,^{\circ}C$.

window of absorption on one hand, and the wide blackbody spectrum on the other hand. The fraction of power emitted by a 650 °C blackbody in the 4.16–4.36 μm range is only 3.5%. As both top and bottom surfaces are emitting, the maximum achievable efficiency is thus 1.75%, which is approached within 90% by our optimal result. To increase this value, we propose to tailor the emissivity of the membrane, mainly in order to spectrally match the absorption of the gas under study.

3.2. Tailored emissivity

In order to increase the optical power emitted by the source at a preset fixed temperature, it is useful to maximize the emissivity of the membrane. Different solutions have been proposed in order to reach a blackbody-like emissivity, including liquid ceramic coatings, silicon grass [17], carbon nanotubes [18] etc. However, when dealing with a single gas measurement, the absorption is spectrally very sharp, and most of the emitted radiation has to be filtered out at the detector. There is thus a major interest in designing efficient sources reaching high emissivity only at the wavelength of interest. This would enable low-consumption sources due to the decrease of radiation losses, as well as a reduced need for external filtering. Salisbury-type configurations [19], gratings [20], photonic crystals [21,22], or more exotic structures [23] can all offer some spectral control over the emissivity. We choose to study Metal Insulator Metal (MIM) plasmonic structures, which have proven their ability to provide a wide-angle, narrow band emission [24–29], while being composed of very thin layers. This last characteristic is critical as these structures have to be deposited on top of the membrane. A dielectric wavelength-scale structure would tend to excessively large thicknesses that would in turn inflict excess thermal inertia. We specifically use MIM resonators, with edges defined by the very shape of the top metallic patches, which are separated from a ground metallic plane by a uniform thin layer of insulating material, as depicted on Fig. 3a. At the resonant frequency, the electromagnetic field is widely enhanced inside the metallic sandwich, due to the excitation of a localized surface plasmon occurring when the lateral patch size is an odd multiple of half the plasmon effective wavelength [30] (Fig. 3b and c), giving rise to a high absorption. Away from the resonance, the structure behaves like a mirror, and is mostly reflecting. We consider in this study a $Pt/Si_3N_4/W$ resonator, which can be deposited on top of the membrane SiO_2 layer and is unaffected by the final etching step used to release the membrane from the substrate.

MIMs were investigated using Rigorous Coupled-Wave Analysis (RCWA)[31], where the electromagnetic field is expanded as a sum of spatial harmonics. This numerical modeling technique is very efficient for periodic systems and amply documented for the case of an externally impinging plane wave. The reflectivity (R) and transmittivity (T) of the structure for a wave of given polarisation, frequency and direction is thus easily computed and according to Kirchhoff law, the emissivity (E) for the same parameters is known to be equal to the absorptivity (A): $E = A = 1 - R - T$. Here, note that R and T comprise the diffracted orders, to safely determine absorption. The simulations are done for all relevant angles, frequencies and both incoming polarizations, and the amount of desired radiation (in the absorption band) and undesirable radiation loss (outside this band) is computed. Optimization leads to a design where the thicknesses of the three layers are identical and equal to 100 nm, and 730 nm-wide square patches are distributed on a 1.5 μm-period array. The dimensions of the patches and the thickness of the dielectric layer are critical parameters, as they influence the resonance both in amplitude and frequency. The design is less sensitive to the thickness of the bottom metallic layer, which just has to be thicker than the skin depth, in order to block

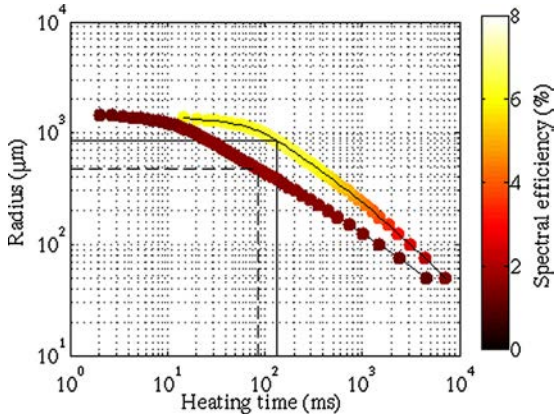

Fig. 4. $R(t_h)$ radius-duration solutions of the constrained thermal equations with $E = 5$ mJ and $T_f = 650$ °C and corresponding spectral efficiency (color). The top brightest curve is the one corresponding to the membrane with the MIM structure, with solid black lines at 135 ms and 850 μm indicating the optimum. The darker bottom curve, provided for comparison, is the one presented on Fig. 2, with dashed lines indicating the original optimum (85 ms and 475 μm).

transmission through the structure. The resulting emissivity features the desired wide-angle resonance at $\lambda \approx 4.25$ μm on the front side (Fig. 3e), and approaches zero on the backside (Fig. 3d). The structure is thus highly reflective from below, avoiding radiative losses toward the substrate. Implementing the angularly integrated emissivities depicted on Fig. 3f (assuming that detection does collect most emitted angles) into the thermal model in Eq. (10), we find the results presented in Fig. 4. The total thickness is now $e = 550$ nm, and average density, heat capacity and thermal conductivity have been updated. The curve corresponding to the original membrane is also provided.

The same kind of behavior is observed, although the MIM structure provides a significant improvement of the spectral efficiency. This is a direct consequence of emissivity tailoring, which strongly reduces radiative losses out of the spectral range of interest. Indeed, integrating the emissivity displayed on Fig. 3c, we find that the optimized source emits 90% of the blackbody radiation in the CO_2 spectral window, while emitting 3 times less total power over the broad blackbody spectrum. As a result, a membrane with a definite radius can be operated with a lower injected electrical current, therefore during a longer time; or conversely a larger membrane can be heated during the same time, yielding improved efficiencies up to 6.5%. This is a considerable improvement, since in the best case scenario, with a perfect "top-hat emissivity", namely $\varepsilon(\lambda) = 1$ for $\lambda \in [4.16\ 4.36]\ \mu$m and $\varepsilon(\lambda) = 0$ elsewhere, we could not get much higher than 16%, as the conductive losses absolute value remains almost constant, and thus caps the achievable efficiency. When temperature and available energy are kept constant, this limit can only be dealt with by modifying the membrane aspect ratio (surface over thickness). Recently, Brucoli et al. [32] studied the thermal behavior of a very large membrane, and demonstrated that the conductive flux can be suppressed under certain conditions. In this case, there would not be any fundamental limit to the efficiency.

4. Conclusion

Thermo-optical mechanisms governing MEMS microhotplates used as infrared sources for gas sensing have been simulated, focusing on the example of CO_2. Their thermal efficiency depends on the ratio between conductive and radiative flux. This ratio can be optimized by choosing adequate membrane radius and heating time, when operating temperature and available energy are respectively enforced by technological (MEMS) and application-derived (battery operation) constraints. We propose a strategy to overcome the limitation induced by the strong mismatch between the sharp gas spectral absorption and the wide blackbody spectrum. In order to limit the spectral radiation bandwidth of the source, we use MIM plasmonic resonators, which provide 90% of the blackbody emission in the desired bandwidth, while emitting on average 3 times less radiation outside this window. Our source allows quadrupling the efficiency compared to the bare membrane while its optimum operation remains in a good range of sizes for practical realization. The proposed membrane is fully CMOS compatible, and is currently under realization for upcoming characterizations.

Acknowledgement

This work was supported by the French National Research Agency (ANR-12-NANO-0005"IDEE").

References

[1] X. Liu, S. Cheng, H. Liu, S. Hu, D. Zhang, A Survey on Gas Sensing Technology, Sensors 12 (2012) 9635–9665, http://dx.doi.org/10.3390/s120709635.
[2] V. Demarne, A. Grisel, An integrated low-power thin-film CO gas sensor on silicon, Sens. Actuators 13 (1988) 301–313, http://dx.doi.org/10.1016/0250-6874(88)80043-X.
[3] D. Bauer, M. Heeger, M. Gebhard, W. Benecke, Design and fabrication of a thermal infrared emitter, Sens. Actuators Phys. 55 (1996) 57–63, http://dx.doi.org/10.1016/S0924-4247(96)01250-2.
[4] U. Khan, C. Falconi, Temperature distribution in membrane-type micro-hotplates with circular geometry, Sens. Actuators B Chem. 177 (2013) 535–542, http://dx.doi.org/10.1016/j.snb.2012.11.007.
[5] U. Khan, C. Falconi, Micro-hot-plates without simply connected hot-spots and with almost-circular temperature distribution, Sens. Actuators B Chem. 185 (2013) 274–281, http://dx.doi.org/10.1016/j.snb.2013.04.098.
[6] G. Saxena, R. Paily, Analytical modeling of square microhotplate for gas sensing application, IEEE Sens. J. 13 (2013) 4851–4859, http://dx.doi.org/10.1109/JSEN.2013.2275951.
[7] S.Z. Ali, F. Udrea, W.I. Milne, J.W. Gardner, Tungsten-based SOI microhotplates for smart gas sensors, J. Microelectromech. Syst. 17 (2008) 1408–1417, http://dx.doi.org/10.1109/JMEMS.2008.2007228.
[8] J. Hildenbrand, C. Peter, F. Lamprecht, A. Kürzinger, F. Naumann, M. Ebert, et al., Fast transient temperature operating micromachined emitter for mid-infrared optical gas sensing systems: design, fabrication, characterization and optimization, Microsyst. Technol. 16 (2010) 745–754, http://dx.doi.org/10.1007/s00542-010-1049-1.
[9] C. Vedel, J.-L. Martin, J.-L. Ouvrier-Buffet, J.-L. Tissot, M. Vilain, J.-J. Yon, Amorphous-silicon-based uncooled microbolometer IRFPA, SPIE (1999) 276–283, http://dx.doi.org/10.1117/12.354529.
[10] P. Barritault, M. Brun, S. Gidon, S. Nicoletti, Mid-IR source based on a free-standing microhotplate for autonomous CO2 sensing in indoor applications, Sens. Actuators Phys. 172 (2011) 379–385, http://dx.doi.org/10.1016/j.sna.2011.09.027.
[11] W.O. Soboyejo, T.S. Srivatsan, Advanced Structural Materials: Properties, Design Optimization, and Applications, CRC Press, 2006.
[12] E. Cozzani, A. Roncaglia, S. Zampolli, I. Elmi, F. Mancarella, F. TAMARRI, et al., Material properties measurement and numerical simulation for characterization of ultra-low-power consumption hotplates, in: Solid-State Sens. Actuators Microsyst. Conf. 2007 TRANSDUCERS 2007 Int., 2007, pp. 1661–1664, http://dx.doi.org/10.1109/SENSOR.2007.4300469.
[13] H.O. Pierson, Handbook of Refractory Carbides & Nitrides: Properties, Characteristics, Processing and Apps., William Andrew, 1996.
[14] F. Cardarelli, Materials Handbook: A Concise Desktop Reference, Springer, 2008.
[15] Tungsten: Properties, Chemistry, Technology of the Elements, Alloys, and ... - Erik Lassner, Wolf-Dieter Schubert - Google Livres, (n.d.). http://books.google.fr/books?hl=fr&id=foLRISkt9gcC&q=density#v=onepage&q=heat&f=false (accessed April 23, 2014).
[16] P. Barritault, M. Brun, O. Lartigue, S. Nicoletti, J. Willemin, J.-L. Ouvrier-Buffet, et al., Low power CO2 NDIR sensing using a micro-bolometer detector and a micro-hotplate IR-source, Sens. Actuators B Chem. (2013), http://dx.doi.org/10.1016/j.snb.2013.03.048.
[17] L. Müller, I. Käpplinger, S. Biermann, W. Brode, M. Hoffmann, Infrared emitting nanostructures for highly efficient microhotplates, J. Micromech. Microeng. 24 (2014) 035014, http://dx.doi.org/10.1088/0960-1317/24/3/035014.
[18] K. Mizuno, J. Ishii, H. Kishida, Y. Hayamizu, S. Yasuda, D.N. Futaba, et al., A black body absorber from vertically aligned single-walled carbon nanotubes, Proc. Natl. Acad. Sci. 106 (2009) 6044–6047, http://dx.doi.org/10.1073/pnas.0900155106.

[19] C.M. Watts, X. Liu, W.J. Padilla, Metamaterial electromagnetic wave absorbers, Adv. Mater. 24 (2012) OP98–OP120, http://dx.doi.org/10.1002/adma.201200674.
[20] M.C. Hutley, D. Maystre, The total absorption of light by a diffraction grating, Opt. Commun. 19 (1976) 431–436, http://dx.doi.org/10.1016/0030-4018(76)90116-4.
[21] I. Celanovic, D. Perreault, J. Kassakian, Resonant-cavity enhanced thermal emission, Phys. Rev. B. 72 (2005) 075127.
[22] C. Blanchard, P. Viktorovitch, X. Letartre, Perturbation approach for the control of the quality factor in photonic crystal membranes: Application to selective absorbers, Phys. Rev. A 90 (2014) 033824, http://dx.doi.org/10.1103/PhysRevA.90.033824.
[23] J. Drevillon, K. Joulain, P. Ben-Abdallah, E. Nefzaoui, Far field coherent thermal emission from a bilayer structure, J. Appl. Phys. 109 (2011) 034315.
[24] M. Diem, T. Koschny, C.M. Soukoulis, Wide-angle perfect absorber/thermal emitter in the terahertz regime, Phys. Rev. B. 79 (2009) 033101, http://dx.doi.org/10.1103/PhysRevB.79.033101.
[25] N. Liu, M. Mesch, T. Weiss, M. Hentschel, H. Giessen, Infrared perfect absorber and its application as plasmonic sensor, Nano Lett. 10 (2010) 2342–2348, http://dx.doi.org/10.1021/nl9041033.
[26] X. Liu, T. Tyler, T. Starr, A.F. Starr, N.M. Jokerst, W.J. Padilla, Taming the blackbody with infrared metamaterials as selective thermal emitters, Phys. Rev. Lett. 107 (2011) 45901.
[27] J.A. Mason, S. Smith, D. Wasserman, Strong absorption and selective thermal emission from a midinfrared metamaterial, Appl. Phys. Lett. 98 (2011) 241105, http://dx.doi.org/10.1063/1.3600779.
[28] I. Puscasu, W.L. Schaich, Narrow-band, tunable infrared emission from arrays of microstrip patches, Appl. Phys. Lett. 92 (2008) 233102–-L1233102, http://dx.doi.org/10.1063/1.2938716.
[29] S. Tay, A. Kropachev, I.E. Araci, T. Skotheim, R.A. Norwood, N. Peyghambarian, Plasmonic thermal IR emitters based on nanoamorphous carbon, Appl. Phys. Lett. 94 (2009) 071113, http://dx.doi.org/10.1063/1.3089225.
[30] J.L. Perchec, Y. Desieres, R.E. de Lamaestre, Plasmon-based photosensors comprising a very thin semiconducting region, Appl. Phys. Lett. 94 (2009) 181104, http://dx.doi.org/10.1063/1.3132063.
[31] M.G. Moharam, T.K. Gaylord, Rigorous coupled-wave analysis of planar-grating diffraction, J. Opt. Soc. Am. 71 (1981) 811, http://dx.doi.org/10.1364/JOSA.71.000811.
[32] G. Brucoli, P. Bouchon, R. Haïdar, M. Besbes, H. Benisty, J.-J. Greffet, High efficiency quasi-monochromatic infrared emitter, Appl. Phys. Lett. 104 (2014) 081101, http://dx.doi.org/10.1063/1.4866342.